Suggested Oxidation State Dependence for the Activity of Submicron Structures Prepared from Tin/Tin Oxide Mixtures

James L. Gole,[†] Alexei V. Iretskii,[‡] Mark G. White,*[,‡] Amanda Jacob,[‡] W. Brent Carter,[§] Sharka M. Prokes,[||] and Ann S. Erickson[‡]

School of Physics, School of Chemical and Biomolecular Engineering, and School of Materials Science and Engineering, Georgia Institute of Technology, Atlanta, Georgia 30332-0100, and Naval Research Laboratory, Surface and Interface Sciences, Code 6862, Naval Research Lab, Washington, DC 20375

Received September 24, 2003. Revised Manuscript Received May 7, 2004

Submicron-sized particles of tin oxide (SnO_x) were prepared via a high-temperature synthesis from the combination of zerovalent tin and tin oxide (SnO) in an inert carrier gas. The size, nature, and relative product yields of the structures produced are dependent upon the synthesis temperature and the ratio of metal/metal oxide in the starting materials. It is suggested that the surface oxidation states of these nanoparticles vary with the ratio of tin to tin oxide and the synthesis temperature so that the product ratio of SnO to SnO_2 and the reactivity of these particles with the phenol hydroxylation reaction could be adjusted. An apparent higher reactivity per unit surface area is observed for the larger submicron particles.

Introduction

We have reported the preparation of nonporous nanoparticles[1] and nanotubes[2,3] from the reaction/interaction of metals/metal oxides at high temperature under inert atmospheres.[2] This technology, while it requires that we heat a select metal/metal oxide mix to high temperature and find an appropriate "sweet zone" in the experimental parameters to efficiently form the desired product,[4] is capable of producing an adsorbent, support, or catalyst by a two-step process that does not require solvents. The effectiveness of this approach has been demonstrated for the synthesis of catalyst supports and conversion agents. We have synthesized silica nanospheres[1,4] as a support for a well-dispersed copper oxide catalyst and hence for the selective conversion of ethanol to acetaldehyde.[5] Recently, we have reported how a silicon/silica based synthesis could be used to tune the surface oxidation state of the formed silica nanospheres.[6] In this paper, we describe our efforts to prepare submicron tin oxide structures in which we are able to manipulate the nature of the products' tin-to-oxygen ratio and their makeup from wires to disks, and for larger and more complex particles ranging in size from tens to hundreds of nanometers. Further, we are able to influence the degree of oxidation and the oxidation state of the tin ion and, in this way, affect the reactivity of the tin oxide products.

Scheme 1. Reaction Sequence for the Hydroxylation of Phenol

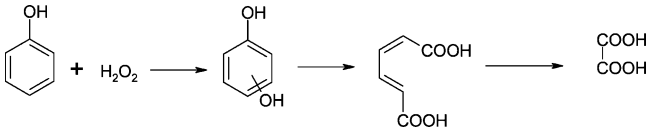

The hydroxylation of phenol has been used as a probe for the activity of titanium silicate (TS-1),[7] supported Fenton's catalysts,[8] and other catalysts (such as zeolites[9]) employing their oxidation activity. The stoichiometric reaction between tin(II) oxide, hydrogen peroxide, and phenol has also been reported.[10] The reaction proceeds[11] in a series path to form oxalic acid through the intermediates hydroquinone, catechol, resorcinol, and muconic acid (Scheme 1).

The stoichiometric hydroxylation reaction occurs only over tin(II) oxide and terminates with the conversion to tin(IV); thus, the activity of the formed tin oxide

* To whom correspondence should be addressed. E-mail: mark.white@chbe.gatech.edu.
[†] School of Physics, Georgia Institute of Technology.
[‡] School of Chemical and Biomolecular Engineering, Georgia Institute of Technolog.
[§] School of Materials Science and Engineering, Georgia Institute of Technolog.
[||] Naval Research Laboratory.

(1) Gole, J. L.; Stout, J. D.; Rauch, W. L.; Wang, Z. L. *Appl. Phys. Lett.* **2000**, *76*, 2346.
(2) Gao, R. P.; Wang, Z. L.; Gole, J. L.; Stout, J. D. *Adv. Mater.* **2000**, *12*, 1938.
(3) Dai, Z. R.; Gole, J. L.; Wang, Z. L.; Stout, J. D. *J. Phys. Chem.* **2001**, *B106,* 1274−9.
(4) Gole, J. L.; Wang, Z. L.; Dai, Z. R.; Stout, J.; Gao, R. P.; White, M. G. *Prog. Coll. Polym. Sci*. **2003**, *281*, 673.
(5) Gole, J. L.; White, M. G. *J. Catal.* **2001**, *204*(1), 249−52.
(6) Gole, J. L.; Shinall, B. D.; Iretskii, A. V.; White, M. G.; Erickson, A. S. *Chem. Phys. Chem.* **2003**, *4,* 1016−21.
(7) Centi, G.; Perathones, S.; Trifiro, F. *J. Phys. Chem.* **1992**, *96*, 2617.
(8) Fairweg, K.; Debellefontaine, H. *Appl. Catal., B* **1996**, *10*, L229.
(9) Allian, M.; Germain, A.; Cseri, T.; Figueras, F. *Heterogeneous Catalysis and Fine Chemicals III* Elsevier Science Publishers: New York, 1993.
(10) Shuvalov, V. F.; Moravskii, A. P. *Dokl. Akad. Nauk SSSR* **1977**, *234* (6), 1402−5.
(11) Barrault, J.; Bouchoule, C.; Echachaoui, K.; Frini-Srasra, N.; Trabelsi, M.; Bergaya, F. *Appl. Catal., B* **1998**, *15*, 269.

10.1021/cm030618i CCC: $27.50
Published on Web 11/12/2004

reactants can be used to infer the surface oxidation state when the characteristic size of the nonporous particles is known.

Experimental Section

Synthesis. The high-temperature technique described previously[1,3] was used to synthesize tin oxide nanostructures in a Lindberg−Blue tube furnace configuration. The temperature inside the synthesis reactor was varied between 1100 and 1150 °C and the time over which the reactants were at this temperature was 12 h.[12] At one end of the tube furnace, for the present tin-based synthesis, ultrahigh purity nitrogen gas enters through an upstream stainless steel end piece, passes through a matched set of zirconia insulators to the central region of the oven and flows, usually at a flow rate of 100 standard cm^3/min, over an alumina crucible which contains the SnO or Sn/SnO source. The use of a layered Sn/SnO reactant greatly increases the formation of SnO_x nanowires and nanoribbons.[3] The total pressure in the inner tube can be changed from 200 to 800 Torr.

The tube furnace downstream end piece is mechanically attached to a water-cooled plate, whose temperature is adjustable (25−40 °C), located at the fringes of the tube furnace hot zone. The entrance and exit regions of the tube furnace are insulated by a machined set of zirconia blocks. A light to dark gray fluffy product is collected on the downstream alumina wall near the point where the temperature is in the range between 450 and 500 °C. Additional products are collected on the cold plate which is positioned ~6 in. into the tube furnace, fronting upstream of the zirconia insulation. This cold plate is maintained at a temperature of 25−40 °C. Conditions can also be adjusted to form a white fluffy product on this coldfinger which can be identified with the virtually complete conversion to SnO_2 and significant nanowire formation. Within this framework the conversion from a black SnO starting material to various stages of SnO_x formation is marked by a transition from dark to light gray and subsequently to a white SnO_2 product upon further oxidation.

When the fluffy gray to gray-black, SnO_x, product is heated slowly to 1100 °C in a centrally located alumina crucible at $P_{total} \approx 200$ Torr under oxidative conditions (1% O_2 seeded in argon) using a concentric nozzle flow over the SnO_x reactant, we observe its complete conversion to a white powder-like product of increased density and which is consistent with bulk SnO_2. Further, if this same fluffy gray product is heated slowly under a reducing atmosphere (Ar/4% H_2 at 1100 °C) it is converted completely to tin metal.

Probe Reaction Conditions. All reactions were conducted in glassware at room temperature under vigorous stirring conditions, so that mass transport would not influence the observed results. A blank run was completed to determine the conversion rates in the absence of the SnO_x solids. For a typical run, 0.021 mmol of phenol (1.7 cm^3 of 11.7 millimolar) was added to 8.4 mmol hydrogen peroxide (9.6 cm^3 of 3 wt %) and this mixture was stirred for 30 min. The initial concentration of phenol was 1.85 millimolar. All of the solids were dried at 110 °C overnight prior to use. Usually, 0.1 g of the prepared tin oxide were added to the reaction mixture, except for one run in which the initial mass of gray, fluffy nanoparticles was increased to 0.157 g. Additional runs were completed with reagent grade stannous oxide and stannic oxide (Aldrich).

Analytical. The liquid samples were withdrawn at desired time intervals and the catalyst was removed immediately, by centrifugation, as the liquid sample was withdrawn. These samples were introduced to an HPLC (Buck Scientific) for analysis of the products that could be detected by a UV−Vis detector. The partitioning column was a C_{18} column obtained from Waters and Associates.

Chemicals. Phenol was purchased from Sigma Aldrich and used without further purification. Authentic samples of hydroquinone, catechol, resorcinol, and muconic acid (*trans, trans*) were purchased from Aldrich as calibration standards for the HPLC. Hydrogen peroxide (3 wt %) was used without further purification. Distilled water was produced on site.

SEM. The as-synthesized products were characterized by scanning electron microscopy (SEM) (Hitachi S-800 FEG) and energy-dispersive X-ray spectroscopy (EDS).

XPS. Samples of tin oxide nanoparticles were examined separately in an XPS instrument (Surface Science model SSX-100 with small spot ESCA spectrometer). Three samples were prepared by combining the following: (I) gray nanostructures (0.04 g) and colloidal gold (0.045 g); or (II) large SnO disks (0.025 g) and colloidal gold (0.023 g); or (III) dense gray nanostructures (0.095 g) and colloidal gold (0.12 g) in a "Wiggle-bug" amalgamator for 20 s on the high setting. The powder was pressed into a lead foil (99.95% metals grade, Alfa Aesar) and this foil was attached to the XPS instrument. These studies, however, for the samples prepared and used in air and in this study, did not provide a definitive indication of a strong surface oxidation state variation.

Raman Spectroscopy. Raman spectroscopy was performed on the samples using a SPEX 1877 triple spectrometer equipped with a Horiba CCD detector. The gray powder-like SnO_x material was placed on a polished Al substrate and the measurements were performed in a nominal backscattering geometry. The excitation light used was the 488-nm line of the Ar^+ laser.

Results

SEM. We observed samples that varied from gray to white, with this range paralleling an increasing SnO_x oxygen content as evidenced by transmission electron microscopy (TEM) and X-ray (EDAX) analysis.[3,13] Among these populations, we readily observed a dependence of the same external appearance on the synthesis reactor conditions and the positions in the reactor where the particles were harvested. The light gray samples harvested from the 450−500 °C region appeared "fluffy" and were of low density; whereas, those harvested from the coldfinger were obviously denser. These samples were also examined for their submicroscopic textures using scanning electron microscopy.[13] We show here the effect on the distribution of nanoparticles obtained by varying the position within the reactor at which the particles are harvested. For product deposition the change from the tube wall to the cold plate varies from a surface temperature close to 450−500 °C to 25−40 °C. Therefore, we expect a more rapid condensation of gaseous products on the cold plate. All of the samples shown here were generated with a starting material composed of layered Sn foil and SnO powder. The products of SnO powders are found to be significantly more oxygen rich and produce primarily larger submicron structures and a minimum of tin oxide (SnO_2) nanowires.[3]

Gray fluffy samples, obtained from heating a reactant mixture formed from interspersed layers of tin (foil) and SnO at a pressure of 400 Torr and harvested from the tube wall (Figure 1), showed an agglomerate structure which also included small SnO diskettes.[3,13] These smaller features displayed some regularity and may, in fact, represent precursors to disk formation. By image

(12) In a select group of experiments, a triple-zone oven system was used in which the central oven region was held at 1300 °C while the side regions were held at 900 °C. The heating procedure was to bring the oven system to temperature, at a rate of between 5 and 10 °C/minute, holding the achieved temperature for a period of 12 h followed by a similar cooling period.

(13) We thank John Stout for assistance in the EDAX and SEM studies.

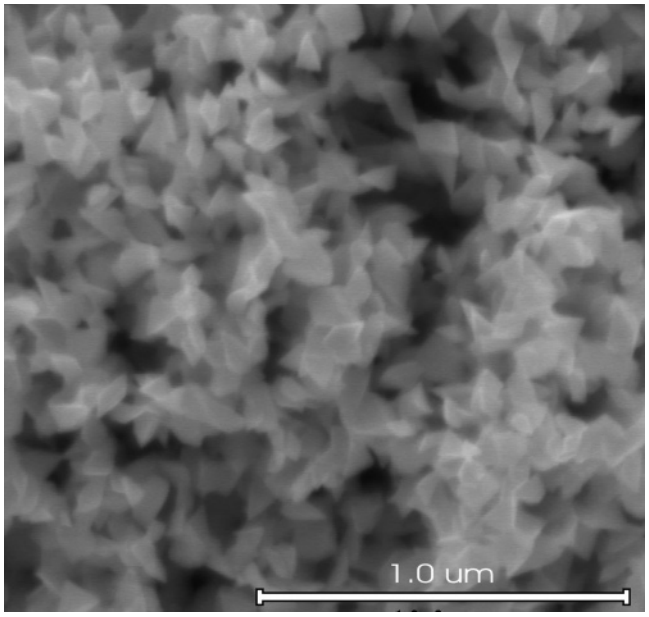

Figure 1. SEM micrograph of fluffy gray samples, showing small regular structures.

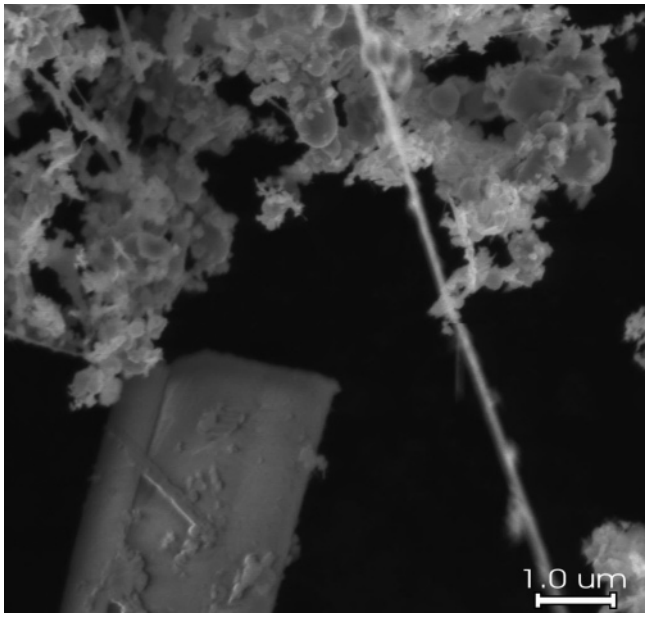

Figure 2. SEM micrograph of fluffy gray samples, showing small diskettes.

analysis we estimate the characteristic size of the smallest SnO_x features at 80 nm or slightly smaller. The SnO_x sample depicted in Figure 2, generated under somewhat different conditions at a lower overall system pressure close to 200 Torr and retrieved from the tube wall (temperature deposition ~450 °C), consisted largely of regular disks having a characteristic diameter which, in some cases, extended to 720 nm, these being identified primarily with SnO, and interspersed with a small component of nanowires.[13] The volume/surface ratio of these particles is estimated to be 240 nm. The dense gray materials, which were collected from the cold plate and whose SEM is exemplified in Figure 3,[13] consisted primarily of diskettes showing characteristic sizes ranging from 1−2.5 μm (Figure 3a), but also larger more complex structures which appeared to represent combinations of disks and extended to 11 μm. The thickness was 1.0−1.3 μm for the largest of these diskettes so that the aspect ratio was ~11. Reagent-grade SnO particles were also examined and appeared as regular tablets, Figure 4,[13] having a much larger volume/area ratio equal to 3 μm and an extent exceeding 12 μm. Fluffy white agglomerates which were interspersed with nanowires and corresponded to to SnO_2 could be formed on the coldfinger using an enhanced SnO powder content in the interspersed Sn/SnO reactant layers heated to 1150 °C. Those nanowires showed a characteristic size, which ranged to below 100 nm, Figure 5.[13]

Phenol Conversion. The hydroxylation of phenol in hydrogen peroxide at 300 K, Figure 6, was completed for the following samples: blank, no solids present; gray fluffy powders consisting of (a) some wire-like structures but dominated by much smaller agglomerated features (Figure 1), and (b) regular disks which range to ~0.72 μm in diameter (Figure 2); (c) dense gray powders consisting of disklike structures ~8−10 μm in diameter (Figure 3); (d) tablets of reagent-grade SnO, >12.2 μm in extent (Figure 4); (e) low-density white powders showing wire-like structures as well as small agglomerates (Figure 5); (f) dense white powder; and (g) dense white powders formed through oxidation of fluffy gray SnO_x samples. Linear equations were fitted to these phenol conversion data at low conversions to define pseudo-first-order rate constants per unit mass of the submicron structures (Table 1). The blank run shows less than a 5% conversion of the substrate in the first 67 h of reaction. The data for the white fluffy powders, the white dense solids, the oxidized samples of the fluffy gray SnO_x powders, and the reagent grade SnO_2 samples indicate a similar, neglible reactivity. In contrast, however, all of the gray samples (SnO_x, $x < 2$) showed a phenol conversion considerably greater than that for the blank runs. The rate constant data, given in Table 1, reflect these trends.

We identified three of the four reaction products by comparison of elution times from the HPLC with authentic samples of hydroquinone, resorcinol, and catechol. These three isomers experienced maxima in yields at reaction times near 40 h and the isomer distribution at this time was 43%, 28%, and 29% for hydroquinone, resorcinol, and catechol, respectively. The apparent yield of an additional unknown peak increased with increasing reaction time.

From these data, we conclude that only the gray samples which consist of SnO_x ($1 < x < 2$) are active and that these samples consist in significant part of Sn(II). In contrast, the white powdered samples all display a surface like that of reagent-grade SnO_2. We have attempted to correct the rate constant data for the differences in size and overall morphology, multiplying the rate constants by the density of the solid and the volume/surface ratio, or characteristic size (Table 1). In this way we attempt to report the intrinsic surface activity of the solids. It is clear that the white powdered samples (dominantly SnO_2) show a reactivity that is very much lower than that of the gray SnO_x powder samples. Within the gray samples, the intrinsic reactivity of the wire-like structures would appear to be exceeded by that of the disks (~0.047−0.058 m^{-2} h^{-1}). We note that the apparent surface activity of the dense gray structures dominated by disks and the reagent-

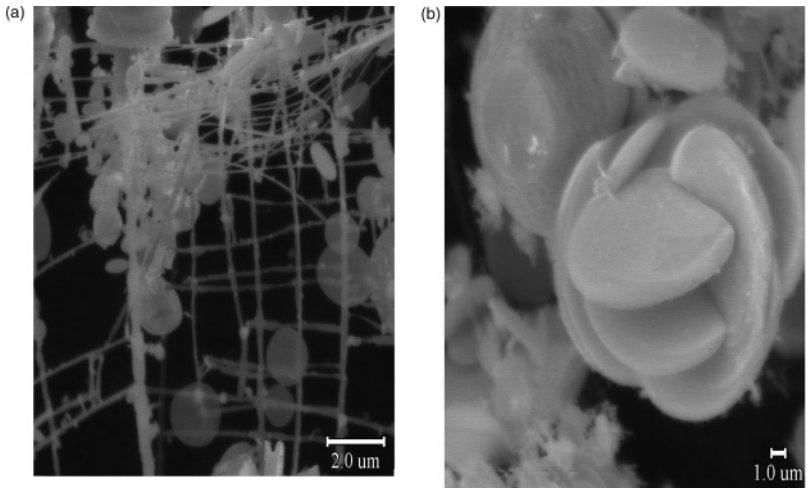

Figure 3. SEM micrograph of dense gray material showing regular disks (a) and detail of larger disks (b) associated primarily with SnO (ref 3).

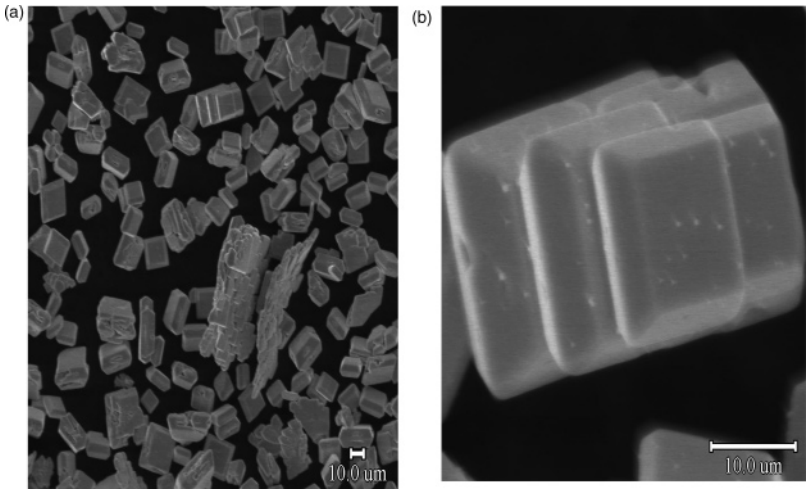

Figure 4. SEM micrograph of reagent-grade SnO showing regular tablets (a) and closer detail of tablets (b).

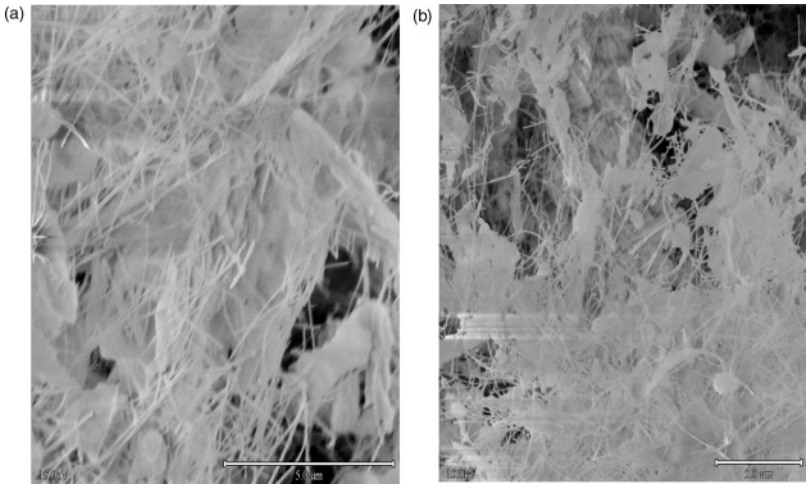

Figure 5. SEM micrograph of fluffy white agglomerates showing wire-like structures (a) and detail (b).

grade SnO tablets was ~27−46 times that of the smaller structures. If the densities of these structures are similar, then this difference in surface activity may be correlated with differences in surface oxidation state suggesting that the gray structures lie intermediate but closer to SnO_2 than they do to SnO.

Results of XPS. The XPS analysis data of the most active structures (fluffy gray) are given in Figure 7a where they are compared with those of an Au internal standard (b). These small submicron structures show a binding energy of 487.1 eV when the Au internal standard shows a binding energy of 83.88 eV. The width of this peak at its half-height was 2 eV. When we calibrate the observed binding energies to those normally expected for Au (83.80 eV), the corrected value of the BE for this sample is 487.1−0.08 eV = 487.02 eV.

Table 1. First Order Rate Constants for Phenol Hydroxylation over Tin Oxide Nanoparticles[a]

nanostructure	k $(g\cdot h)^{-1}$	d μm	$k\rho d$ $(m^2\cdot h)^{-1}$	μmol Sn^{2+}/g	monolayers Sn^{2+} used
fluffy gray nanostructures; XPS BE= 487 eV; width = 2.0 eV	0.089	0.083	0.0495	20.7	2.6
fluffy gray nanostructures, repeat	0.085	0.083	0.0473	20.7	2.5
gray disks; XPS BE = 487 eV; width = 1.8 eV	0.036	0.24	0.0579	7.2	2.7
dense gray nanostructures (coldfinger) XPS BE = 486.9 eV; width = 2.1 eV	0.024	0.45	0.0724	3.8	3.8
SnO reagent	0.011	3	0.221	0.57	17.4
fluffy white nanostructures	0.0065				
dense white nanostructures	0.0053	1	0.0355		
dense white nanostructures, oxidized	0.0028				
SnO_2 reagent	0.0033				
blank*	0.00039				
SiO_2 nanostructures[6]	0.267	0.0068	0.00375		

[a] k = mass specific rate constant, d = characteristic dimension of nanoparticles, volume/surface ratio, and ρ = density of nanoparticles.

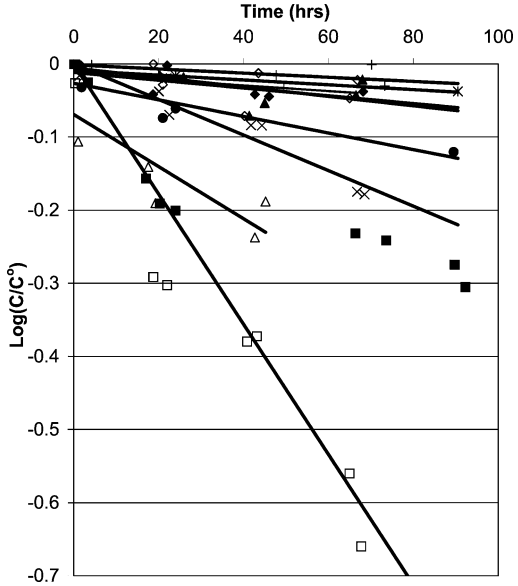

Figure 6. Phenol hydroxylation activity for tin oxide nanostructures: ♦, fluffy white run 6/7; ■—, fluffy gray, run 10/9, 0.1 g; □, run 10/9, 0.157 g; ▲, —dense white, run 10/11; ×, dense gray, run CF 6/7; *, SnO_2 reagent, white; ●, SnO, reagent, gray; +, dense white, oxidized in crucible, run 6/25; ◊, blank run, no solids; △, —gray disks, 10/11. Reaction temperature = 298 K, 0.1 g of solid for all runs (except for 10/09 second run where 0.157 g of solid was used), excess H_2O_2 (3 wt % in water), initial [phenol] = 1.85 mM.

In a like manner we correct the BE values for the additional samples to show Sn $3d_{5/2}$ BE energies of 487.09 eV (gray nanodiscs, sample II), and 486.86 eV (dense, gray nanostructures, sample III). The width of these peaks at their half-heights were 1.75 eV (sample II) and 2.13 eV (Sample III). Further tests were run and no charging was observed in these samples.

Raman Spectroscopy. Nanowires and ribbons, similar to those shown in Figures 2 and 3, were examined by Raman spectroscopy, Figure 8, to determine which phases were present. A consideration of the spectrum in Figure 8a and its correlation with data from the literature suggests that we should assign the peaks at 480, 632, and 776 cm^{-1} to SnO_2;[14] whereas the peak at 213 cm^{-1} can be assigned to the SnO phase.[15] The peaks at 130 and 176 cm^{-1} may be attributed to a transition oxide phase, SnO_x, where $1 < x < 2$.[14,15] In contrast, the Raman spectrum for the white powdered samples of Figure 5, taken with a converted apparatus that does not extend below 175 cm^{-1}, is shown in Figure 8b. It is evident that this sample which does not show the 213 cm^{-1} feature mainly consists of SnO_2, as demonstrated in the figure, and virtually no suboxides are evident. This sample shows a reactivity which is much lower than that of the gray SnO_x sample whose Raman spectrum is shown in Figure 8a.

Discussion

The submicron-sized materials generated in this study are similar to those reported in the literature generated by the "gas-phase condensation" method.[16] This approach has been used by Jimenez, et al to produce nanosized tin oxides, 8−10 nm in diameter, from starting materials of either Sn, SnO, or SnO_2.[17] In subsequent papers, these authors reported using the gas-phase condensation method to deposit SnO_x nanostructures on silica or on highly oriented pyrolytic carbon,[18] and magnesia.[19] The nanostructures developed in these studies were similar to those we report here, albeit smaller. In particular, these researchers show that nanoparticles containing SnO_2 are the major component of a synthesis initiated with SnO. Moreover, they report that exposure of this material to room-temperature air converts Sn and SnO at the surface of the particles they generate to SnO_2 even though XRD data demonstrates significant Sn and SnO in the bulk phase.[15] Dai et al.[20] describe the morphology of tin oxide diskettes showing a stoichiometry near SnO that were formed by a process similar to that shown here where the starting materials were either SnO or SnO_2. They report a typical diameter of 8−10 μm for their diskettes with an aspect ratio of 15. Moreover, they showed that these diskettes were the tetragonal SnO structure (*P4Inmm*). While some of our diskettes are nearly twice as large as those reported by Dai et al., the aspect ratio

(14) Geurts, J.; Rau, S.; Richter, W.; Schmitte, F. J. *Thin Solid Films* **1984**, *121*, 217.
(15) Sangaletti, L.; Depero, L. E.; Allieri, B.; Pioselli, F.; Comini, E.; Sberveglieri, G.; Zocchi, M. *J. Mater. Res.* **1998**, *13*, 2457.
(16) Gunter, B.; Kaumpman, A. *Nanostruct. Mater.* **1992**, *1*, 27. Geiter, H. *Adv. Mater.* **1992**, *4*, 474.
(17) Jimenez, V. M.; Gonzalez-Elipe, A. R.; Espinos, J. P.; Justo, A.; Fernandez, A. *Sens. Actuators* **1996**, *B 31*, 29−32.
(18) Jimenez, V. M.; Gonzalez-Elipe, A. R.; Espinos, J. P.; Justo, A.; Fernandez, A. *Surf. Sci.* **1996**, *350*, 123−35.
(19) Jimenez, V. M.; Espinos, J. P.; Gonzalez-Elipe, A. R. *Surf. Sci.* **1996**, *366*, 556−63.
(20) Dai, Z. R.; Pan, Z. W.; Wang, Z. L. *J. Am. Chem. Soc.* **2002**, *124* (29), 8673−80.

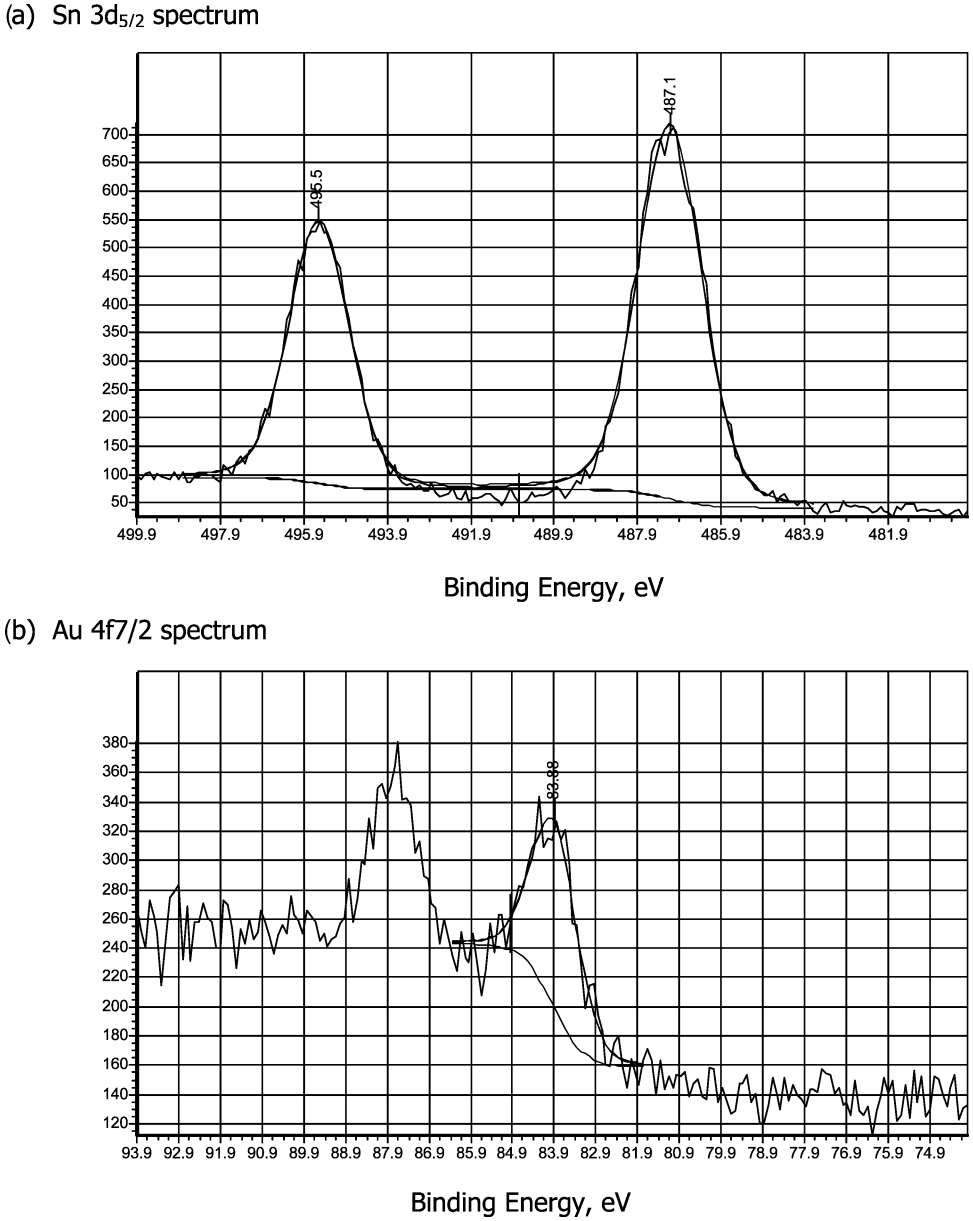

Figure 7. X-ray photoelectron spectra of tin oxide nanostructures: Sn $3d_{5/2}$ (a), and Au $4f_{7/2}$ (b).

of the diskettes we describe here is very close to that of those prepared by these authors. Others report the ease with which metallic tin can be oxidized by room-temperature air and also report difficulty in reducing the surface tin oxide back to metallic tin.[21] These two results are relevant to our attempts to characterize, by XPS, the submicron tin oxide structures we have generated (vide infra).

We can compare our hydroxylation results to those reported by others[10] for the homogeneous reaction of phenol over Sn(II) ion, which is known to occur by the following redox mechanism:

$$Sn^{2+} + 2HOOH \rightarrow 2OH\bullet + Sn^{4+} + 2OH^{-} \quad (1)$$

By this mechanism, the oxidation of each Sn^{2+} ion by H_2O_2 produces 2 OH radicals that can react subsequently with 2 phenol molecules. Only divalent tin is active for this stoichiometric reaction. We show (Figure 6) that the initial activity of the gray SnO_x ($1 \leq x < 2$) structures is unchanged even when the initial amount of sample is increased from 0.1 to 0.157 g; however, the ultimate phenol conversion (0.8) obtained over the heavier sample was about 1.6 times the conversion obtained over the lighter sample (0.51) at 100 h. This result suggests that the number of surface Sn(II) cations corresponds to the limiting reagent for this stoichiometric reaction between H_2O_2 and Sn(II) and that the reaction stops when all available Sn(II) is converted to Sn(IV). When the number of Sn(II) cations becomes the limiting reagent, then the phenol conversion versus time will no longer obey first-order kinetics in phenol. Thus, we see systematic departures from first-order behavior at longer reaction times (Figure 6). We have observed a similar result for the phenol hydroxylation over silica nanospheres.[6]

We may estimate the maximum number of surface Sn^{2+} cations by considering the crystal structure of SnO

(21) Epling, W. S.; Mount, C. K.; Hoflund, G. B. *Appl. Surf. Sci.* **1998**, *134*, 187–93.

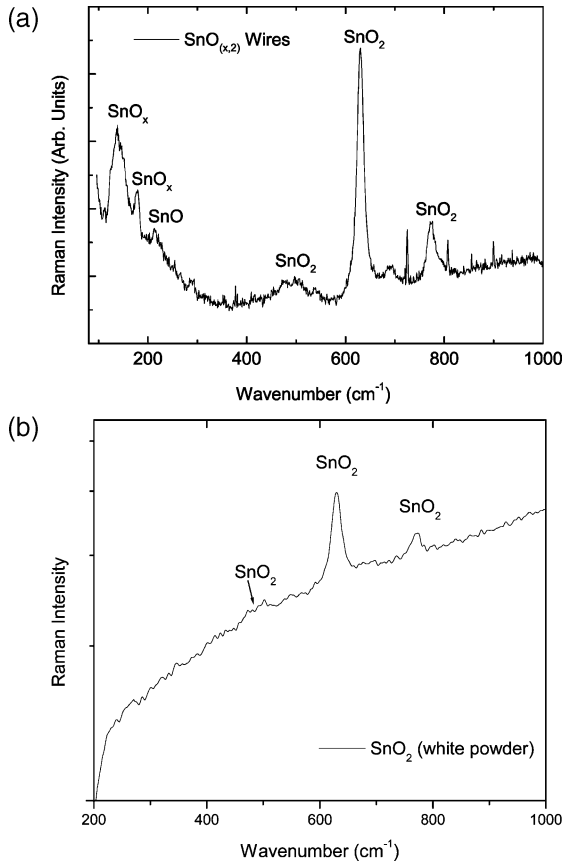

Figure 8. Raman spectroscopy of (a) tin oxide wires and ribbons, (b) SnO_2 white powder.

(tetragonal with $a = 3.796$ and $c = 4.816$ Å). If we assume that the surface structure of our materials is similar to the surface structure of crystalline SnO, and if we use the observations of Dai et al. that the flat sides of the diskettes were the (**001**) plane, then we estimate that the maximum surface density of Sn^{2+} is $6.94 \times 10^{+18}$ cations/m^2. This surface cation density may be used to calculate the μmoles of surface Sn^{2+} cations per gram of solid (Table 1, column 5) from a consideration of the volume/surface area ratio, d (Table 1, column 3) and the density of the solid (~6.7 g/cm^3). This number can be compared to the number of phenol molecules converted over each solid per unit mass so as to determine the equivalent number of Sn^{2+} cation monolayers required for this conversion (Table 1, column 6). These results suggest that the amount of phenol converted exceeded the amount of divalent tin in the outermost surface layer. Thus, the surface layer of tin cations must have been regenerated by some mechanism. Either (1) the submicron structures are porous,[22] thus allowing the reaction to proceed past the external boundary by diffusion of reactants into the interior, or (2) the solid is a complex shell/core structure[23] where the surface region contains oxidized Sn^{4+} cations that are reduced by some mechanism using Sn^{2+} in the interior core region as the reductant. Vincent[24] showed that nonstoichiometric tin oxide conducted electricity as a result of the mobility of electrons from Sn^{2+} to Sn^{4+} sites. Alterkop et al.[25] modeled the air-annealing process in SnO_x films by assuming that electrons could be transported between the interior and the surface of the film and that the SnO phase provided oxygen vacancies that act as charge donors.

The mass-specific rate constants for the hydroxylation of phenol over these samples would appear to reflect not only the intrinsic reactivity of the surface but also the surface/volume ratio and the density of the nanostructures. We have attempted to correct these rate constants for differences in the surface/volume ratio by multiplying the mass-specific rate constants (column 2, Table 1) by the volume/surface ratio (column 3, Table 1) so as to determine the rate constant corrected for size effects. If we assume that the densities of these submicron structures are the same and equal to an average density[26] of 6.7 g/cm^3, then the corrected rate constants (column 4, Table 1) may be compared to assess the relative reactivity of the solids per unit surface area. These data suggest that the white submicron structures show no significant activity over that observed for a blank run in which no solids were present. This result is consistent with a surface rich in tin (IV) which is known to be unreactive toward the phenol hydroxylation reaction. The gray structures all show activity toward the phenol hydroxylation reaction for which the activity per unit surface area depends on the size of the structure. The smallest structures (~80 nm) show the lowest activity per unit surface area (0.0473−0.0495 $h^{-1}m^{-2}$), the gray disks ~240 nm diameter show a reactivity of 0.0579 $h^{-1}m^{-2}$, and the dense gray structures (4.5 μm) show a surface reactivity of 0.0724 $h^{-1}m^{-2}$. The SnO reagent grade standard (tablets ~3 μm) shows an intrinsic reactivity of 0.221 $h^{-1}m^{-2}$. In the same table we can compare the mass-specific and area-specific rate constants for the phenol hydroxylation reaction over the much smaller silica nanospheres, which we reported earlier.[6] It is not surprising that these tin oxide nanostructures are more reactive than the silica nanostructures based upon reactivity per unit surface area. The activity per unit surface area suggests that the larger particles show a higher intrinsic activity than the smaller particles. We now endeavor to use a traditional model for reaction and diffusion in porous media[26,27] to determine if that model can explain the initial reactivity per unit mass data. One such model for isothermal pellets shows that the rate constant per unit mass obeys the following simple equation:

$$k = \tanh(d)/[d] + \text{constant}$$

For small values of d the rate becomes a constant value, and for large values of d the rate scales with $^1/_d$. Thus, this model predicts a log−log relationship with inverse particle size for the asymptotic solution to the model when diffusion of reactants into the pores influences the reaction rates (i.e., when d is large). To test

(22) Yoo, K. S.; Cho, N. W.; Song, H. S.; Jung, H. J. *Sens. Actuators* **1995**, *B24−25*, 474.
(23) Shek, C. H.; Lai, J. K. L.; Lin, G. M.; Zheng, Y. F.; Liu, W. H. *J. Phys. Chem. Solids* **1997**, *58* (1), 13−17.
(24) Vincent, C. A. *J. Electrochem. Soc.* **1972**, *119*, 515.
(25) Alterkop, B.; Parkansky, N.; Goldsmith, S.; Boxman, R. L. *J. Phys. D: Appl. Phys.* **2003**, *36*, 552−8.
(26) This density is the arithmetic average of the density of SnO (6.446 g/cm^3) and SnO_2 (6.95 g/cm^3). Densities for tin oxides are from Dean, J. A., Ed.; *Lange's Handbook of Chemistry, 12th ed.*; McGraw-Hill: New York, 1979.
(27) Satterfield, C. N. *Mass Transfer in Heterogeneous Catalysis*; MIT Press: Cambridge, MA, 1970.

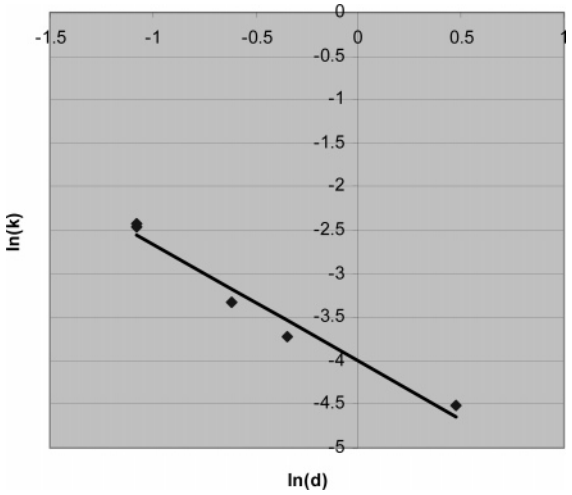

Figure 9. Application of the effectiveness factor model to explain data of initial rates versus particle size.

this theory as an explanation of our data, we plot the observed rate constant/mass (k, column 2) versus the characteristic size (d, column 3) as shown in Figure 9. The data would have to fall on a line for this model to successfully interpret the data at low values of the diameter, and, moreover, this model predicts an invariant behavior at low values of the diameter. We show on the same figure a regression line for which the slope is -1.35 ± 0.45 at the 95% confidence level. This slope should be -1 according to theory, and, moreover, any departure from linearity according to the theory should define a curve having a negative second derivative (concave downward). From a consideration of Figure 9, it is obvious that the data, when processed according to this manner, show a systematic deviation from linearity. Random errors in the rate constant alone would not produce this systematic deviation from linear behavior on the log−log chart. This deviation from the expected behavior suggests that a simple, isothermal model for reaction and diffusion in a porous solid cannot explain our data.

The surface-region oxidation state(s) of the samples can be interrogated using XPS. The binding energies of the zero, divalent, and tetravalent states of tin, recently reported in the literature, are 484.9, 486.4, and 486.8 eV,[28] 487.0 eV, respectively.[29] Others report the following binding energies for tin oxide species: SnO (486.2 eV); SnO_2 (486.4 eV); and the transitional oxide, Sn_3O_4 (485.2 eV).[18] Tsunekawa et al.[29] have studied the effect of an alkaline versus acidic surface environment on their nanoparticle structures upon tin oxidation and found that the oxidation state for alkaline particles increases to that of bulk tin oxide. This is the same result that is suggested by our phenol hydroxylation data. The XPS analysis of our samples containing much larger particles, prepared and studied in air, suggests that we examine binding energies and the width of the XPS peaks at their half-heights to learn more about the average oxidation states of tin. Our XPS data indicate approximately the same BE (~487 eV) for the Sn ion in samples I (fluffy, gray submicron structures) and II (gray submicron disks) and a slightly smaller BE for sample III (dense, gray disklike structures, 486.9 eV), but the widths of these peaks were slightly different. Sample III was the widest at 2.13 eV, sample I was slightly smaller at 2.0 eV, and sample II was the smallest at 1.75 eV. While these results suggest that the samples show the same BE within the error of the binding energies reported for SnO_2 (BE = 486.8 and 487.0 eV), the samples may contain other oxidation state(s) of tin, owing to the width of the peaks, which may be under the shoulders of the principal peak. That is, for the observed peak at 487 eV with a width of nearly 2 eV at half-height, SnO (BE = 486.4 ev) could be present and "hiding" under the shoulder of the principal peak. These XPS results certainly do not contradict the Raman spectra that clearly show both divalent and tetravalent tin in our samples.

Shek et al.[29] showed how Mossbauer spectroscopy could be used to interrogate the slow oxidation process of small SnO_x particles in ambient air. They prepared ultrafine particles of tin oxide (vide supra) showing different sizes (10, 25, and 50 nm) which were then characterized by Mossbauer spectroscopy as a function of exposure time to ambient air so as to determine how the oxidation state of the solid changed with time. Since Mossbauer spectroscopy is a volume-averaging technique, they could determine the kinetics for oxidizing the solid ($Sn^{2+} \rightarrow Sn^{4+}$) from the exterior to the interior as a function of time and particle size. They showed how the tin cations in the smallest particles (10 nm) were very quickly converted from stannous ions to stannic ions, and how this conversion rate was smaller for the larger particle sizes (25 and 50 nm). They postulated a shell/core model where the shell was a disordered phase rich in Sn^{4+}, and the core phase was an ordered phase which contained tin in lower oxidation states (2+ and 0).

This shell/core model appears to explain well the data of XPS and Raman spectroscopy. Moreover, the shell/core model could explain the data of phenol conversion and reactivity where the number of phenol molecules reacted exceeded the maximum number of Sn^{2+} cations in the surface layer. Furthermore, the increasing reactivity per unit surface area for the larger particles could be explained by a model where the surface cations are kept in a reactive state by the migration of electrons from the core to the surface. Migration of electrons in nonstoichiometric tin oxide is noted for solids even at room temperature.

Conclusions

We believe that the tin oxide submicron structures show a thin oxide film containing both Sn(II) and Sn(IV) which covers a core containing lower oxidation states of tin. This conclusion is supported by both the XPS data, which characterize only the surface region to a depth of ~10 nm, and by the Raman spectroscopy data, which characterizes the entire solid. The larger particles show higher intrinsic reactivity *per unit surface area* than the smaller particles, probably as a result of surface renewal from the bulk to provide Sn(II) as needed for reaction. Therefore, we report an unusual effect of particle size that results in the small particles having a lower, intrinsic, surface reactivity. However,

(28) Wagner, C. D.; Davis, L. E.; Riggs, W. M. *Surf. Interface Anal.* **1986**, *2*, 53.
(29) Tsunekawa, S.; Kang, J.; Asami, K.; Kawazoe, Y.; Kasuya, A. *Appl. Surf. Sci.* **2002**, *201*, 69−74.

the small size of the smallest particles, with their attendant higher surface area/volume ratio, makes them appear to be the most reactive species *on a per unit mass basis*. Finally, all samples show a thin surface oxide film containing Sn(IV) that is unreactive to the phenol hydroxylation reaction covering a core material richer in the tin oxide(s) of lower oxidation state that are the reactive species for this reaction. This unreactive shell/reactive core model was also advanced by us to explain the data characterizing silica nanostructures.[6]

Acknowledgment. We acknowledge the support of A.S.E. and A.J. by the National Science Foundation under the auspices of the NSF-REU program.

CM030618I